Supporting information

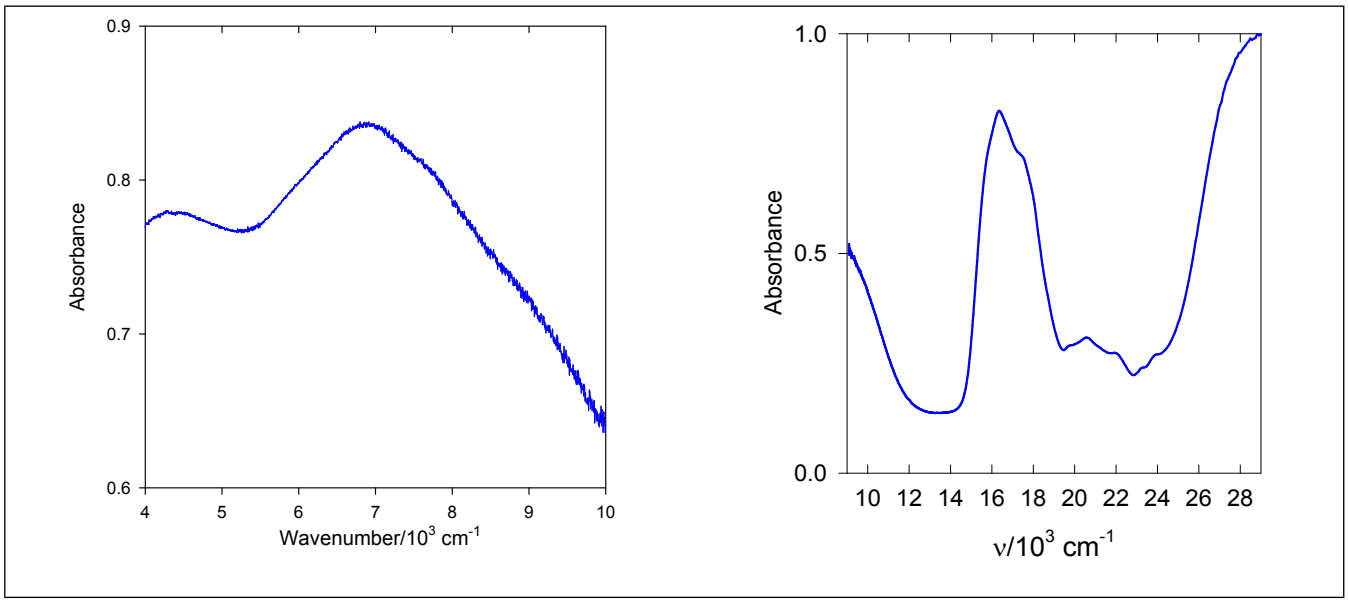

Figure S1. Electronic spectrum of **1** measured in the Nujol mull. Left – NIR region, right – UV/Vis. Absorbances are different due to different thickness of the samples.

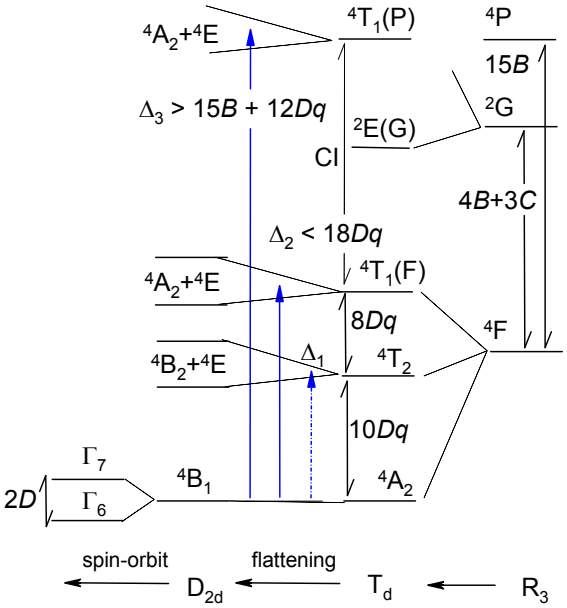

Figure S2. Energy levels diagram relevant to **1**.

Table S1. Calculated absorption spectrum by CASSCF (NEVPT2 diagonal energies)

States	Energy (cm-1)	Wavelength (nm)	fosc	T2 (D**2)	TX (D)	TY (D)	TZ (D)
0(0)-> 1(0) 4	**4648.6**	2151.2	0.000000153	0.00007	-0.00508	0.00665	0.00000
0(0)-> 2(0) 4	4648.6	2151.2	0.000000153	0.00007	-0.00665	-0.00508	0.00000
0(0)-> 3(0) 4	**5490.0**	1821.5	0.000000000	0.00000	0.00000	0.00000	0.00000
0(0)-> 4(0) 4	**8319.9**	1201.9	0.000055634	0.01420	-0.00000	-0.00000	-0.11916
0(0)-> 5(0) 4	**8621.4**	1159.9	0.000064577	0.01591	-0.12056	0.03702	0.00000
0(0)-> 6(0) 4	8621.4	1159.9	0.000064576	0.01591	-0.03702	-0.12056	0.00000
0(0)-> 7(0) 4	**20352.0**	491.4	0.000347072	0.03621	-0.06351	-0.17938	-0.00000
0(0)-> 8(0) 4	**20352.1**	491.4	0.000347071	0.03621	0.17938	-0.06351	0.00000
0(0)-> 9(0) 4	**20878.6**	479.0	0.000413542	0.04206	-0.00000	0.00000	-0.20509

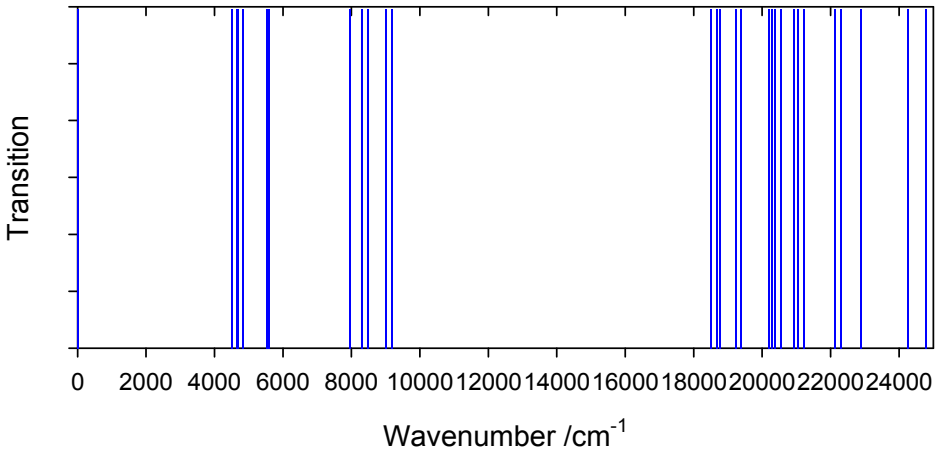

Figure S3. Calculated electronic transitions (spin-orbit corrected).

Table S2. Individual contributions to D-tensor

Block	Mult	Root	D	E
0	4	0	0.000	0.000
0	4	1	**12.465**	-8.660
0	4	2	**12.465**	8.660
0	4	3	**-21.252**	-0.000
0	4	4	-0.000	0.000
0	4	5	0.003	-0.003
0	4	6	0.003	0.003
0	4	7	0.000	0.000
0	4	8	0.000	-0.000
0	4	9	0.000	0.000
1	2	0	0.000	-0.000
1	2	1	-0.000	-0.000
1	2	2	-0.068	-0.067
1	2	3	-0.068	0.067
1	2	4	0.000	-0.000
1	2	5	0.000	0.000
1	2	6	**-3.156**	-1.393
1	2	7	**-3.156**	1.393
1	2	8	**6.09**8	0.000
1	2	9	-0.073	0.073
1	2	10	-0.073	-0.073
1	2	11	**-0.186**	-0.118
1	2	12	**-0.186**	0.118
1	2	13	-0.000	-0.000
1	2	14	**0.405**	0.000
1	2	15	0.000	0.000
1	2	16	0.000	0.000
1	2	17	-0.000	0.000
1	2	18	-0.000	-0.000
1	2	19	0.000	0.000
1	2	20	0.000	0.000
1	2	21	-0.003	-0.003
1	2	22	-0.003	0.003
1	2	23	**1.326**	0.000
1	2	24	**-0.500**	-0.480
1	2	25	**-0.500**	0.480
1	2	26	0.000	0.000
1	2	27	0.000	-0.000
1	2	28	0.000	0.000
1	2	29	**-0.142**	-0.136
1	2	30	**-0.142**	0.136
1	2	31	**0.246**	0.000
1	2	32	0.000	-0.000
1	2	33	-0.003	0.001
1	2	34	-0.003	-0.001
1	2	35	0.000	-0.000
1	2	36	0.000	0.000
1	2	37	0.048	-0.000
1	2	38	-0.023	0.023
1	2	39	-0.023	-0.023

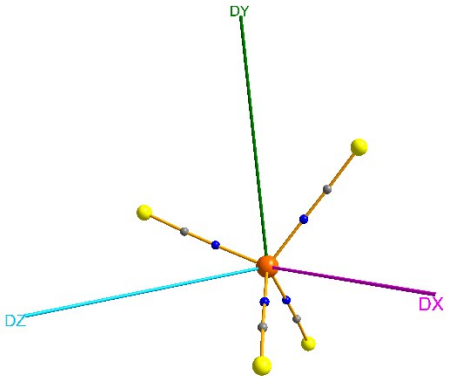

Figure S4. Calculated main axes of the D-tensor.

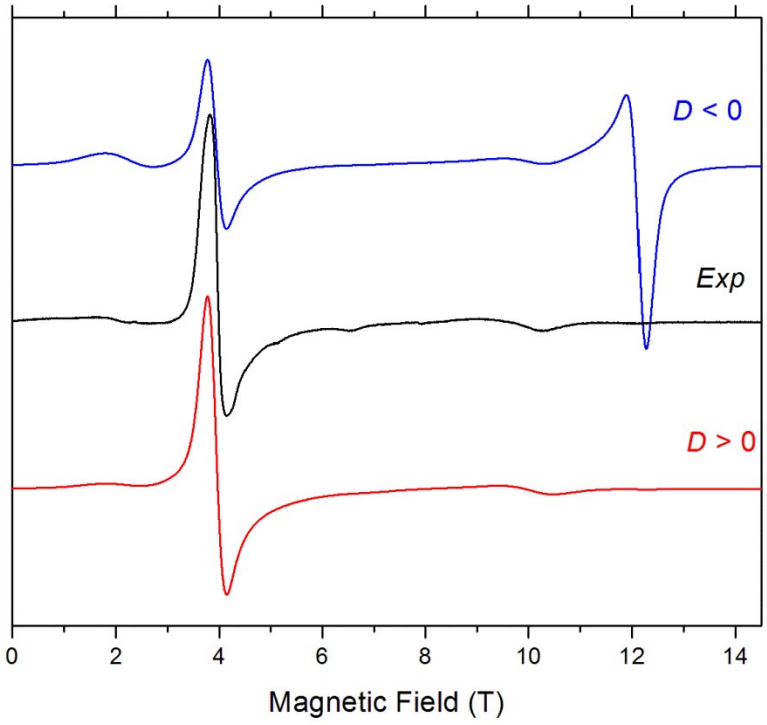

Figure S5. A 10 K EPR spectrum of $HgCo(NCS)_4$ at 214 GHz (black trace) and its simulations (colored traces) using the following spin Hamiltonian parameters: $|D| = 5.39$ cm^{-1}, $E = 0$, $g_{\|} = 2.2$, $g_{\perp} = 2.14$. Blue trace: $D < 0$; red trace: $D > 0$.

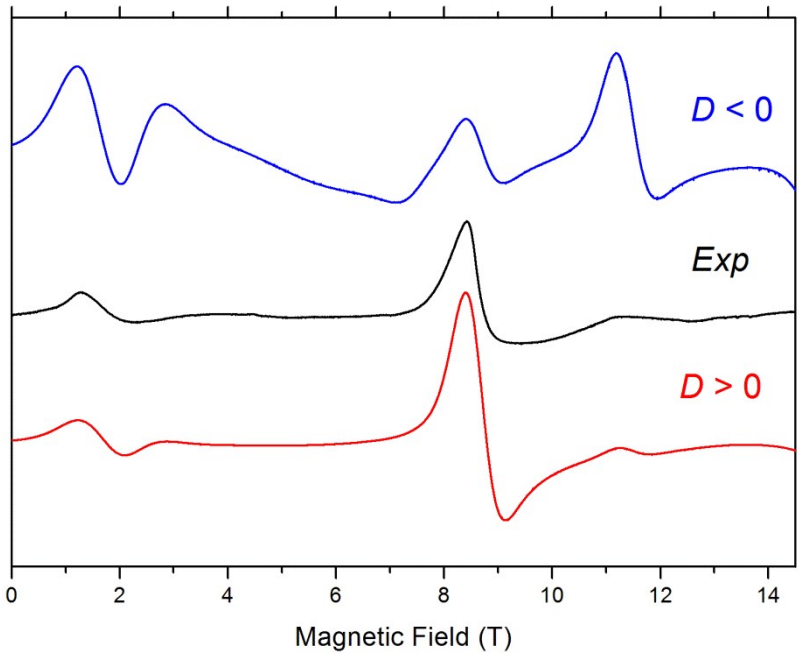

Figure S6. A 10 K EPR spectrum of $HgCo(NCS)_4$ at 406 GHz (black trace) and its simulations (colored traces) using the following spin Hamiltonian parameters: $|D| = 5.39$ cm^{-1}, $E = 0$, $g_{iso} = 2.2$. Blue trace: $D < 0$; red trace: $D > 0$.

AC susceptibility data

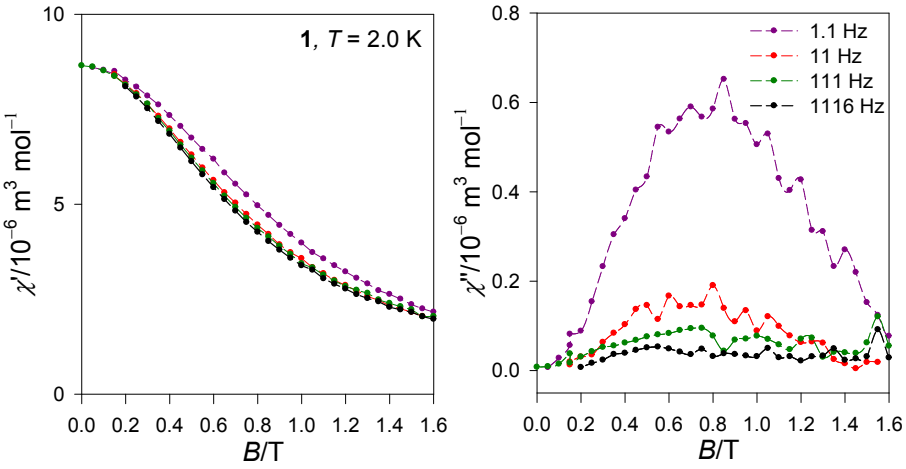

Figure S7. Field dependence of the AC susceptibility for **1** at $T = 2.0$ K.

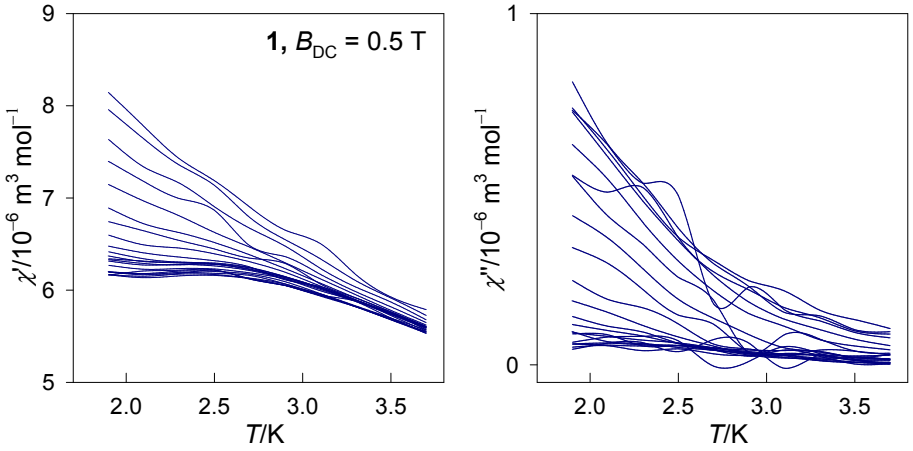

Figure S8. Temperature dependence of the AC susceptibility for **1**.

A quantitative analysis is based upon an extended Debye model with two relaxation processes
a) in phase component

$$\chi'(\omega) = \chi_S + (\chi_{T1} - \chi_S)\frac{1 + (\omega\tau_1)^{1-\alpha_1}\sin(\pi\alpha_1/2)}{1 + 2(\omega\tau_1)^{1-\alpha_1}\sin(\pi\alpha_1/2) + (\omega\tau_1)^{2-2\alpha_1}}$$

$$+(\chi_{T2} - \chi_{T1})\frac{1 + (\omega\tau_2)^{1-\alpha_2}\sin(\pi\alpha_2/2)}{1 + 2(\omega\tau_2)^{1-\alpha_2}\sin(\pi\alpha_2/2) + (\omega\tau_2)^{2-2\alpha_2}}$$

b) out of phase component

$$\chi''(\omega) = (\chi_{T1} - \chi_S)\frac{(\omega\tau_1)^{1-\alpha_1}\cos(\pi\alpha_1/2)}{1 + 2(\omega\tau_1)^{1-\alpha_1}\sin(\pi\alpha_1/2) + (\omega\tau_1)^{2-2\alpha_1}}$$

$$+(\chi_{T2} - \chi_{T1})\frac{(\omega\tau_2)^{1-\alpha_2}\cos(\pi\alpha_2/2)}{1 + 2(\omega\tau_2)^{1-\alpha_2}\sin(\pi\alpha_2/2) + (\omega\tau_2)^{2-2\alpha_2}}$$

for $\omega = 2\pi f$; χ_T – isothermal susceptibility (low-frequency limit), χ_S – adiabatic susceptibility (high-frequency limit). The fitting procedure contains 7 free parameters and a combined functional $F = w_1 \cdot R(\chi') + w_2 \cdot R(\chi'')$ is to be minimized (R_i – relative error, w_i – weight of the component).

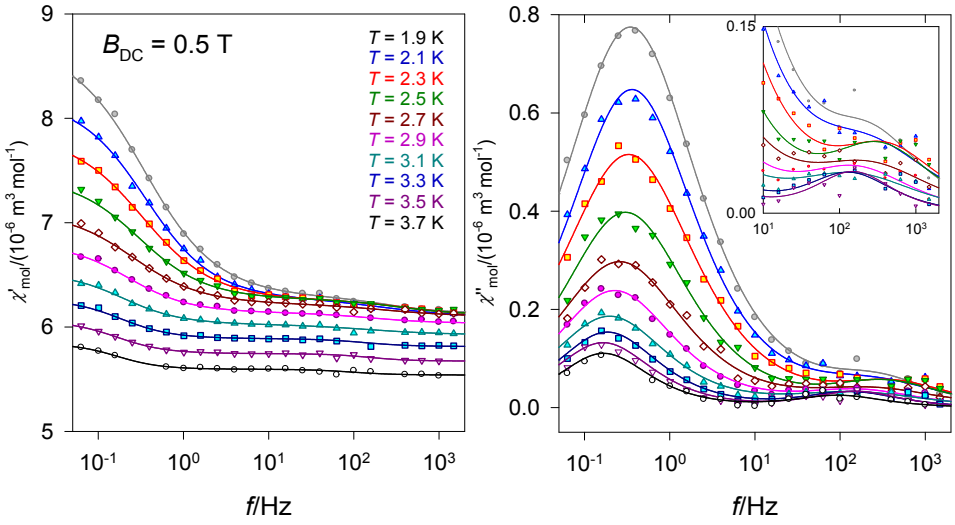

Figure S9. Dependence of the AC-susceptibility components upon the frequency of the AC field and temperature at $\boldsymbol{B_{DC}}$ **= 0.5 T**. Solid lines – calculated. The fitted parameters along with their standard deviations are listed in Table S3.

While the first (low-frequency) maximum is recovered by the fitted parameters well, the characteristics of the second (high-frequency) maximum are only tentative (the signal is too low and noisy). Note, the AC susceptibility data are taken with very low amplitude of the oscillating field B_{AC} = 0.38 mT and thus the data are influenced by the eddy currents and other instabilities of the superconducting magnet that rise with B_{DC}.

Table S3. Parameters of the two-set Debye model for **1** (two relaxation processes) at B_{DC} = 0.5 T. [a]

T/K	$R(\chi')$/%	$R(\chi'')$/%	χ_S	χ_{TLF}	α_{LF}	τ_{LF} /s	χ_{THF}	α_{HF}	τ_{HF} /10^{-3} s	x_{LF}
1.9	0.31	2.2	6.13(2)	8.59(5)	.28(1)	0.46(1)	8.73(3)	.18(16)	0.58(17)	.95
2.1	0.32	3.2	6.10(3)	8.05(6)	.25(1)	0.44(1)	8.21(3)	.30(18)	0.63(26)	.92
2.3	0.26	4.1	6.11(2)	7.73(5)	.27(1)	0.48(1)	7.86(2)	.20(17)	0.38(13)	.92
2.5	0.31	6.9	6.12(2)	7.30(5)	.25(2)	0.53(3)	7.44(3)	.20(18)	0.47(16)	.89
2.7	0.27	6.9	6.10(2)	7.00(5)	.26(3)	0.62(4)	7.11(3)	.29(20)	0.65(30)	.88
2.9	0.17	4.8	6.04(1)	6.71(3)	.22(2)	0.71(3)	6.81(2)	.23(12)	0.97(23)	.87
3.1	0.22	6.5	5.93(1)	6.43(3)	.19(3)	0.81(5)	6.52(2)	.29(15)	1.05(36)	.84
3.3	0.17	8.5	5.81(1)	6.19(2)	.13(3)	0.86(5)	6.27(1)	.10	1.18(27)	.84
3.5	0.16	13	5.67(1)	6.00(2)	.12(4)	0.96(7)	6.06(1)	.04	1.04(21)	.82
3.7	0.23	13	5.54(1)	5.76(1)	.01	0.88(7)	5.82(1)	.001	1.15(30)	.80

[a] Susceptibility in 10^{-6} m^3 mol^{-1} (SI units). $R(\chi')$ and $R(\chi'')$ – discrepancy factors of the fit for the in-phase and out-of-phase susceptibility; standard deviations in parentheses.

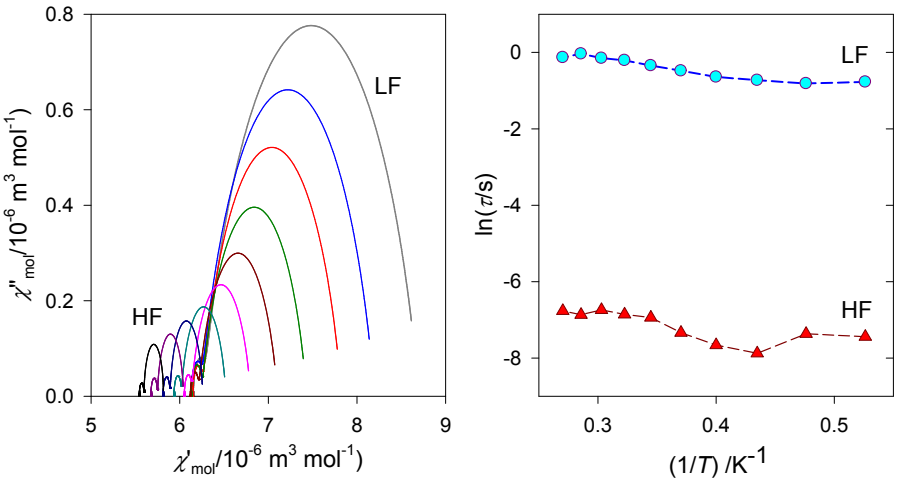

Figure S10. Arrhenius-like plot (left) based upon fitted data. LF – low frequency, HF – high frequency data.

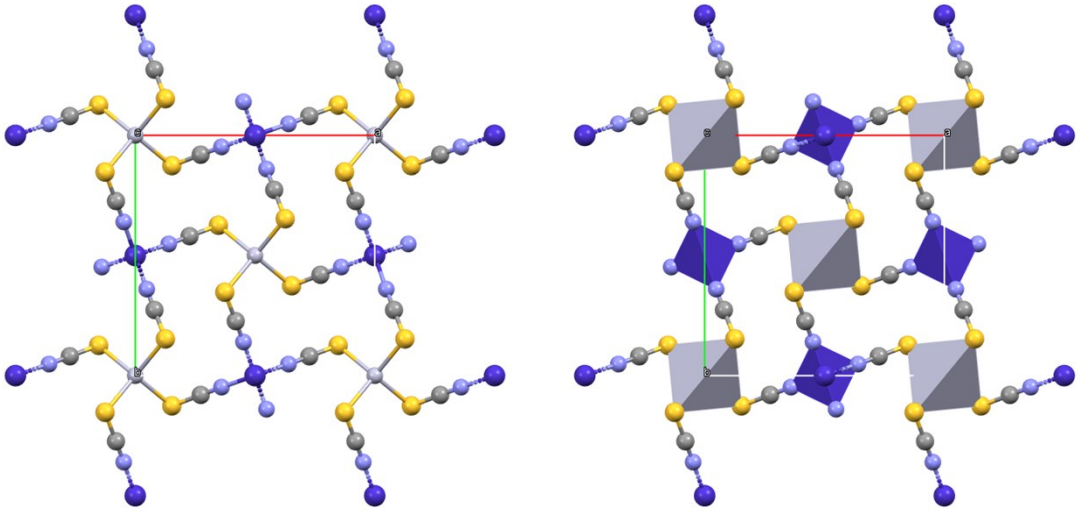

Figure S11. View of the unit cell of **1** showing the 3D structural motif [ICSD 36062].
J.W. Jeffery, K.M. Rose, Acta Crystallographica, Section B: Struct.Crystallogr.Cryst.Chem., 1968, 24, 653, DOI: 10.1107/S0567740868002980

Table S4. Magnetic data and parameters for $HgCo(NCS)_4$

Technique	Detail	μ_{eff} / μ_B	g_z, g_{iso}	g_x	θ [K]	D/hc [cm^{-1}]	Ref.
Gouy	80-300 K	4.33 (300 K) 4.18 (90 K)			–10 *		S1
Gouy		4.32			–4		S2
Faraday	5.8-293 K				+2		S3
Faraday					+2.4 -1.0 -0.95		S4
SQUID					–1.1		S4
VSM	B = 1.0 T		2.24, 2.21, 2.22(rec.)		–1.86	+19	S5
SQUID	B = 0.008 – 0.38 T	4.37 (30-100 K)	2.26		–0.62		S6
SQUID	B = 0.5 T	4.36 (293 K)	2.22		–0.32	$2D$ = +10.6 *	S7
SQUID	B = 0.1 T	4.36 (295 K)	2.223	2.292	zj = –0.114	+3.86	This work
HFEPR			2.13(8)	2.16(5)		+5.23(10) E = 0.046(2)	This work
Ab initio			2.211	2.264		+3.41	This work
Generalized crystal field	$10Dq$ = 5000 cm^{-1}		2.252	2.294		+3.65	This work

* Corrected data to usual convention.

(S1) Figgis, F. N.; Nyholm, R. C. 61. Magnetochemistry. Part II. The temperature-dependence of the magnetic susceptibility of bivalent cobalt compounds. *J. Chem. Soc.*, **1959**, 338-345.

(S2) Cotton, F. A.; Goodgame, D. M. L.; Sacco, M. Magnetic Studies of High-spin Cobaltous Compounds. VII. Some Thiocyanate Complexes. *J. Am. Chem. Soc.* **1961**, 83, 4157-4161.

(S3) Rade, H.-St. Temperature dependence of the magnetic susceptibility of mercury tetrathiocyanatocobalt. *J. Phys. Chem.* **1973**, 77, 424.

(S4) Bunzli, J.-C. G. Comment of the use of $HgCo(NCS)_4$ as susceptibility standard. *Inorg. Chim. Acta.* **1979**, 36, L413-L414.

(S5) Brown, D. B.; Crawford, V. H.; Hall, J. W.; Hatfield, W. E. Standards for magnetic measurements. A comparison and a proposal for the use of tetramethylethylenediammonium tetrachlorocuprate(II). *J. Phys. Chem.* **1977**, 81, 1303–1306.

(S6) O' Connor, C. J.; Sinn, E.; Cukauskas, E. J.; Deaver, B. S. Low temperature magnetic properties and antiferromagnetic interactions of the magnetic susceptibility calibrant $HgCo(NCS)_4$. *Inorg. Chim. Acta*, **1979**, 32, 29-32.

(S7) Nelson, D.; ter Haar, L. W. Single-crystal studies of the zero-field splitting and magnetic exchange interactions in the magnetic susceptibility calibrant mercury cobalt-thiocyanate ($HgCo(NCS)_4$), *Inorg. Chem*. **1993**, *32*, 182-188.

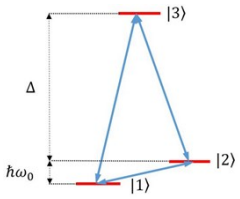

Modelling of the two-set susceptibility

A three-level model [L. T. A. Ho and L. Chibotaru, Phys. Rev. 2016, B94, 104422] brings the AC susceptibility components (in the original symbolism)

$$\chi'(\omega) = \frac{1}{T}\frac{c}{1+2c}\left(m_{11}^2 \frac{1}{1+\omega^2\tau_2^2} + \frac{m_{33}^2}{1+2c}\frac{1}{1+\omega^2\tau_3^2} \right)$$

$$\chi''(\omega) = \frac{1}{T}\frac{c}{1+2c}\left(m_{11}^2 \frac{\omega\tau_2}{1+\omega^2\tau_2^2} + \frac{m_{33}^2}{1+2c}\frac{\omega\tau_3}{1+\omega^2\tau_3^2} \right)$$

The relaxation rates involving the direct and Orbach terms are

$\lambda_2 / \Gamma_0 = a_n T + \Gamma_0 / (c-1) = A(\Delta / k_B T)^{-1} + 1/(c-1)$, $\tau_2^{-1} = \lambda_2$

$\lambda_3 / \Gamma_0 = (2c+1)/(c-1)$, $\tau_3^{-1} = \lambda_3$

with $A = a(\Delta / k_B)/\Gamma_0$ and $c = \exp(\Delta / k_B T)$; matrix elements of the magnetic momentum $m_{ii} = \langle i | \hat{m}_z | i \rangle$.

The direct term is field-dependent $\lambda_{direct} = A_{direct} B^n T = a_n T$ with typical values of $n = 2 - 4$.

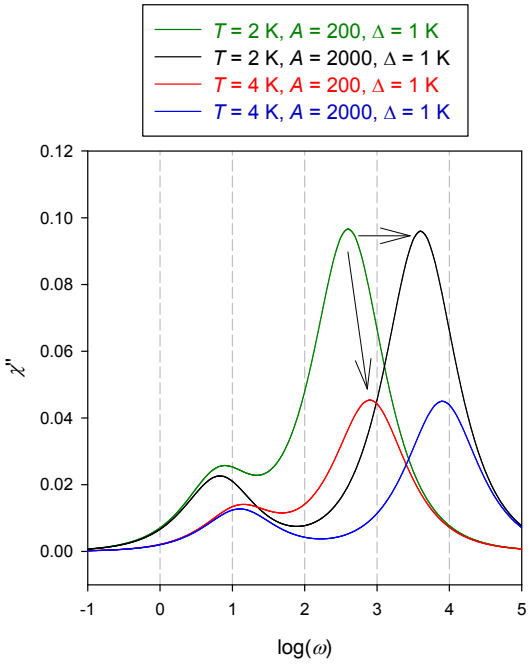

For $m_{33} = m_{11} = 1$

a) Effect of field: $A = 200 \rightarrow 2000$, green *vs* black; peak separations increases;

b) Effect of temperature, $T = 2 \rightarrow 4$ K, green *vs* red and black *vs* blue; peak maxima decrease and move to higher frequency.

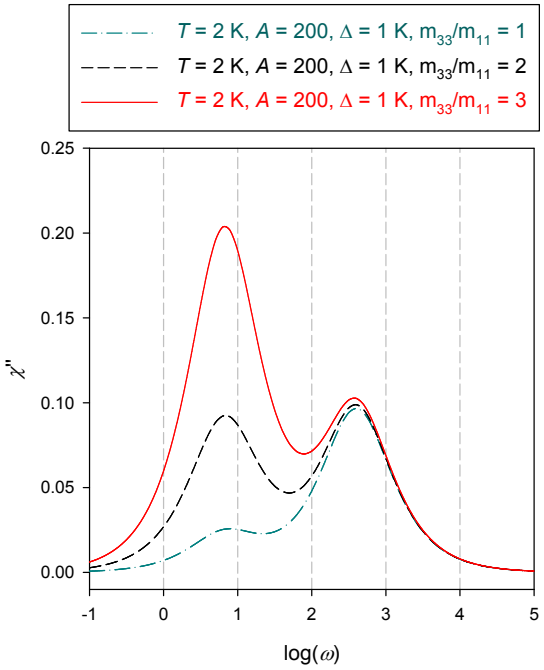

Effect of matrix elements: m_{33} / m_{11}: low-frequency peak increases.

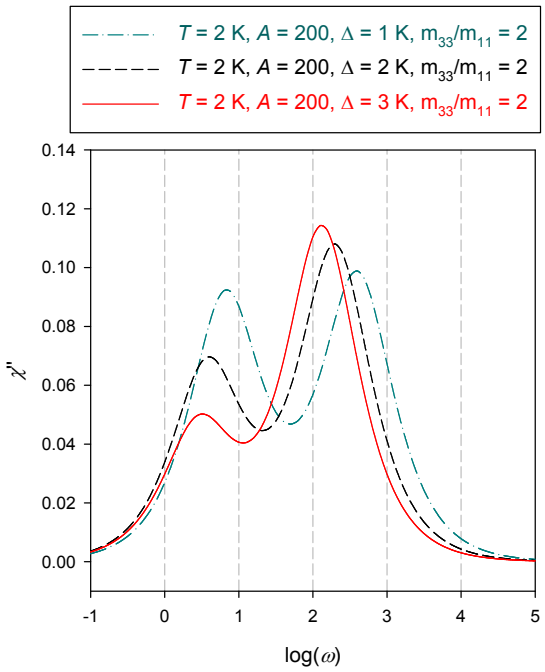

Effect of the energy gap Δ:
a) peak movement to lower frequencies;
b) peak intensity changes

Figure S12. A modelling of the out-of-phase AC susceptibility using a three-level model.